Flow between Two Coaxial Rotating Cylinders with a Highly Water-Repellent Wall

Keizo Watanabe, Tsukasa Takayama, Satoshi Ogata, and Seiji Isozaki
Graduate School of Engineering, Tokyo Metropolitan University, Tokyo, Japan 192-0397

The torque and velocity profile of a flow between two coaxial cylinders with a highly water-repellent wall were measured experimentally. Two kinds of highly repellent wall were tested to clarify the surface condition effect of the cylinder on laminar drag reduction with fluid slip. The results of torque measurement showed that laminar drag reduction does not occur for a highly water-repellent wall with no fine grooves at the wall surface. Fluid slip of Newtonian fluids was clarified by measuring the velocity profile close to the highly water-repellent wall in a Couette flow by a tracer method for flow visualization. The maximum slip velocity is less than 20% of the wall velocity of the rotating inner cylinder. The result of the drag reduction ratio for the torque was calculated by applying to the slip velocity, and agrees with the experimental result quantitatively. Consequently, the gas trapped in the fine grooves plays an important role in laminar drag reduction with respect to fluid slip. From the flow visualization of laminar Taylor–Couette flow, the intervals of Taylor cells become slightly irregular in the case of the cylinder with a highly water-repellent wall. The calculation result for the Taylor cell applying the fluid slip boundary condition agrees with the experimental result.

Introduction

Drag reduction can be achieved in several ways, and the techniques related to these have been investigated during the past several decades. One technique is to dissolve high-molecular polymer or surfactant in a liquid. This gives rise to the well-known Toms effect (Toms, 1948), wherein the friction of a dilute polymer solution in a turbulent pipe flow decreases in comparison with that of the solvent alone. Recently studies have focused on drag reduction with surfactant solutions because there is no degradation with these, in contrast to polymer solutions. Surfactant solutions, then, are more practical in recirculating heat-supply systems.

Another method of drag reduction is to change the condition of the surface. A well-known example is the use riblets, which resemble the fine grooves on the surface of sharkskin. Generally speaking, the target of these methods is to modify the structure of the turbulent flow adjacent to the surface.

On the other hand, drag reduction can occur in laminar flow in a pipe when the surface is a highly water-repellent wall, as we reported recently (Watanabe et al., 1999). In that work, it was shown that the friction factor could be reduced by up to 18%. The basic material in the highly water-repellent coating is fluorine-alkane-modified acrylic resin with added hydrophobic silica. The coating, initially liquid, is left overnight in air on the pipe wall. The wall surface has a fractal-type structure with many fine grooves. An analytical result was obtained by applying Navier's hypothesis (Navier, 1816) for fluid slip, and good agreement was obtained between theory and experiment. Subsequently, drag reduction with the coating was reported for an enclosed rotating disk (Watanabe and Ogata, 1998; Ogata and Watanabe, 1999) and coaxial rotating cylinders (Watanabe and Akino, 1999). However, fluid slip could not be confirmed in these experiments because the necessary measurements of velocity near a wall could not be made using a conventional technique.

The purpose of this study is to further understand the effect of a highly water-repellent wall on laminar drag reduction by using PIV to make velocity measurements. Shear flow between two coaxial rotating cylinders has a simple exact solution to which velocity measurements can be compared. Thus, using PIV, we obtained velocity profiles between two coaxial cylinders in which the inner cylinder was rotated and the outer cylinder was at rest, for different surfaces on the inner cylinder.

Correspondence concerning this article should be addressed to K. Watanabe.

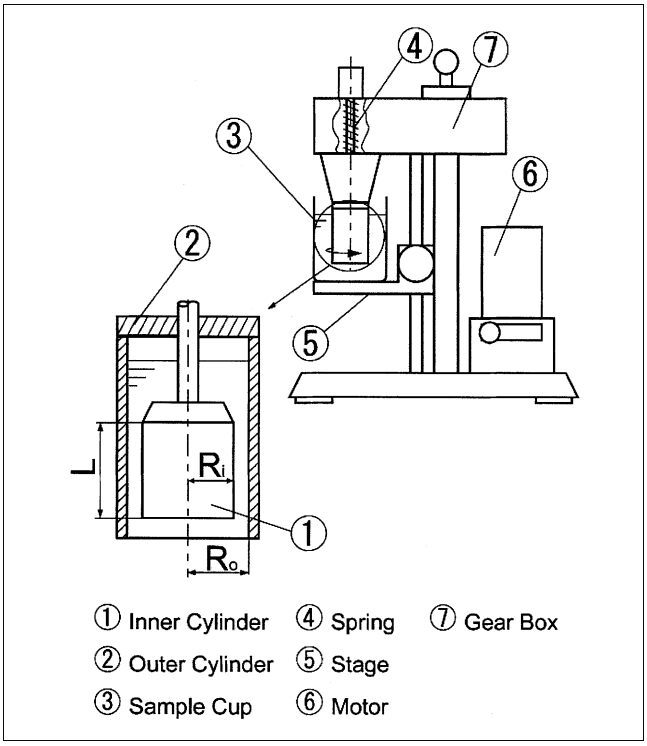

Figure 1. Experimental apparatus for torque measurement.

Experimental Apparatus and Method

Figure 1 shows the experimental apparatus for torque measurement. The rotational speed of the outer cylinder was varied from 0.9 rpm to 600 rpm, and the ratio of the radii of the inner and outer cylinders was $\kappa = 0.932$. The test fluids were 60 wt %–80 wt % glycerin solutions, the properties of which are listed in Table 1. The torque acting on the stationary inner cylinder was measured by means of a torsion spring. The surface of the inner cylinder was smooth or was coated with a highly water-repellent material. Two kinds of coatings were applied in this experiment. For the first coating (wall #1), many fine particles of polytetrafluoroethlen (PTFE) were bonded to the surface; for the second (wall #2), a mixture of fluorine-alkane-modified acrylic resin and hydrophobic silica was applied and left overnight in air. Micrographs of the two surfaces, and the shapes of water droplets on these surfaces are shown in Figures 2 and 3, respectively. It is apparent that these walls are so water repellent that the contact angles are almost 150°C. Although the angles are the same for the two materials, Figure 2 shows that the surface geometries are different. The apparatus for the flow visualization study is shown in Figure 4. In this apparatus the inner cylinder is rotated and the outer is at rest, in contrast to the apparatus for torque measurements (Figure 1). The rotational speed of the inner cylinder was varied from 6 rpm to 31 rpm. A laser beam and cylinder were used to create a horizontal or vertical sheet of light for the flow visualization. The PIV tracer particles were hollow glass beads with a diameter of 10 μm and an apparent specific gravity of 1.1. Images created by bead movements were captured by a digital camera. Several inner cylinders were used in this study, and their dimensions and that of the outer cylinder are listed in Table 2.

Table 1. Physical Properties of the Aqueous Solution of Glycerin

Conc. (%)	Density ρ (kg/m^3)	Viscosity μ (Pa·s)	Kinematic ν (m^2/s)	Temp. T (°C)
60	1,157	13.1×10^{-3}	11.3×10^{-6}	15
70	1,185	28.1×10^{-3}	23.7×10^{-6}	15
80	1,212	72.2×10^{-3}	59.6×10^{-6}	16

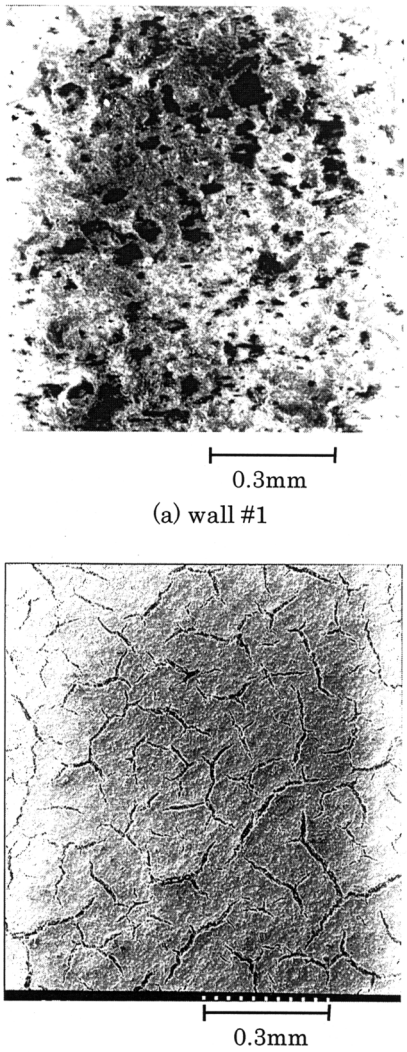

Figure 2. Micrographs of the highly water-repellent wall.

Results and Discussion

Moment coefficient of inner cylinder

If we assume fluid slip at the wall, the shear stress on the inner cylinder is obtained by applying Navier's boundary condition (Navier, 1816) $\tau_w = \beta V_s$, where τ_w is the wall shear stress, V_s is the tangential slip velocity at the inner wall, and

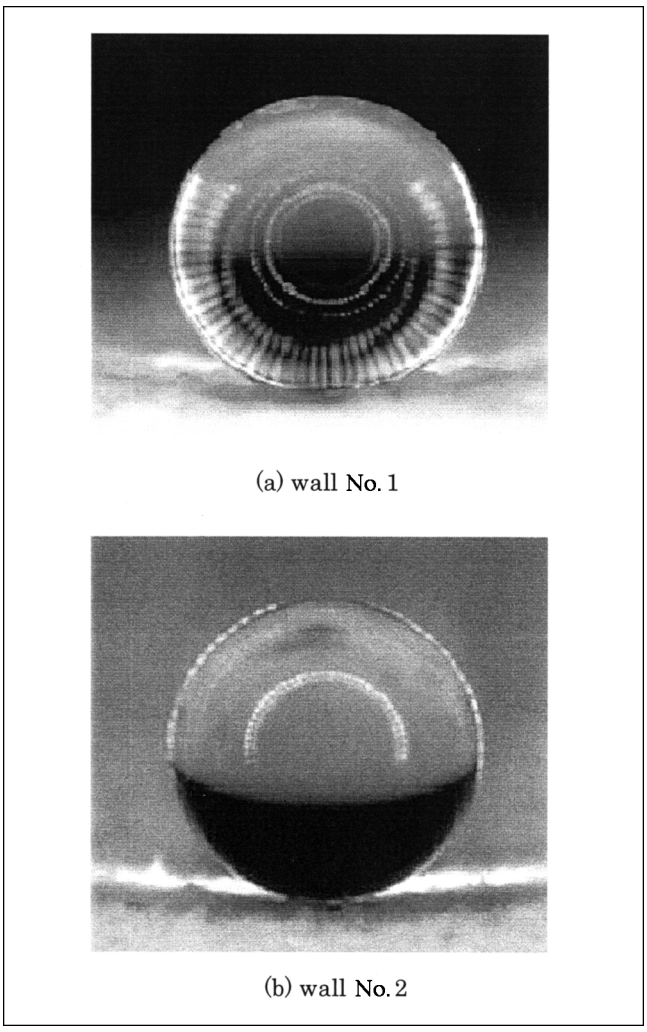

Figure 3. Shapes of a drop of water on the wall.

β is the sliding coefficient

$$C_m = \frac{16\kappa^2}{(\kappa+1)^4}\left(1-\frac{2}{\frac{\beta R_0}{\mu}\kappa(1-\kappa^2)+2}\right)\Bigg/ R_\omega \qquad (1)$$

When slip does not occur, $\beta = \infty$, and the preceding equation reduces to

$$C_m = \frac{(1-\delta/R_0)^2}{\left(1-\delta/R_0+(\delta/2R_0)^2\right)^2}\Bigg/ R_\omega \qquad (2)$$

Measurements of torque on the inner cylinder with smooth wall, Teflon wall, and highly water-repellent walls No. 1 and No. 2, and for three fluids, are presented in Figure 5. In terms of the torque coefficient, they have 95% confidence limits; hence for the 60% solution in Figure 5a, for example, the true values lie within $\pm 1.97\%$ of the plotted values.

Figure 5a shows that drag reduction does not occur for wall No. 1, because the data are the same as for a smooth stainless steel wall. However, as Figure 5b shows, with wall

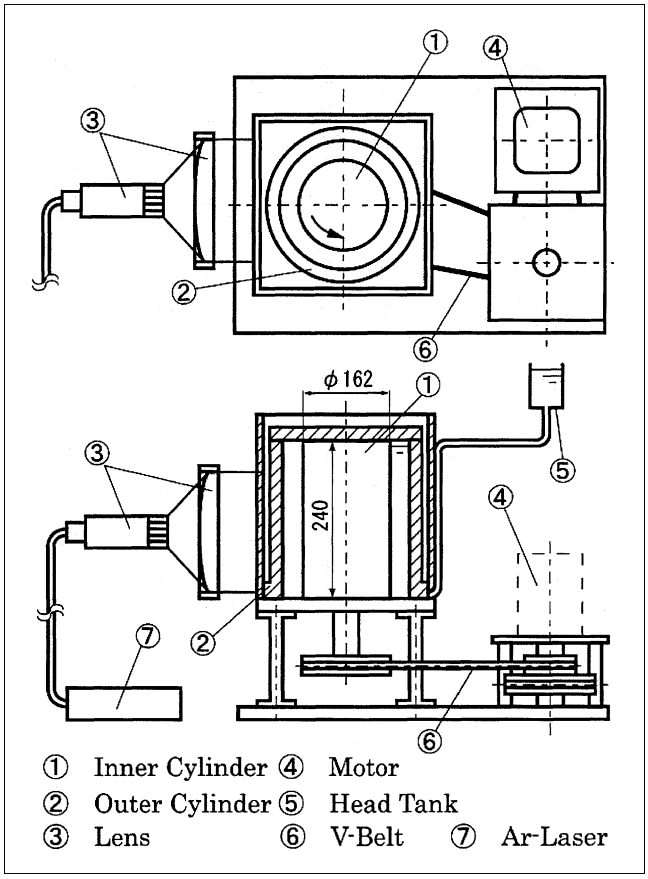

Figure 4. Experimental apparatus for flow visualization.

No. 2 there is drag reduction, up to a maximum of about 12% for the 80 wt. % glycerin solution. In the previous study on flows in a coated pipe (Watanabe and Udagawa 2001), we pointed out the existence of the air trapped in the fine grooves, which is the reason why the drag reduction occurs on the surface. This fact does not contradict the experimental result that the drag reduction does not occur in highly water-repellent wall No. 1, even though the wall surface is highly repellent.

In the previous study on flow in a coated pipe (Watanabe et al., 1999), it was thought that drag reduction occurred because of fluid slip. The coating in that study had fine grooves. Thus, the present study suggests that fluid slip does not occur at wall No. 1 because that wall does not have fine grooves, even if the surface is highly repellent.

Velocity Measurements

The path lines of tracer particles are shown in Figure 6, as an example of the photographs obtained for making PIV measurements. Velocity profiles were determined by measur-

Table 2. Dimensions of Cylinders for Flow Visualization

No.	R_i (mm)	R_o (mm)	κ	δ (mm)	L (mm)	Γ
1		87	0.931	6		40
2	81	96.5	0.839	15.5	240	15.5
3		120	0.675	39		6.15

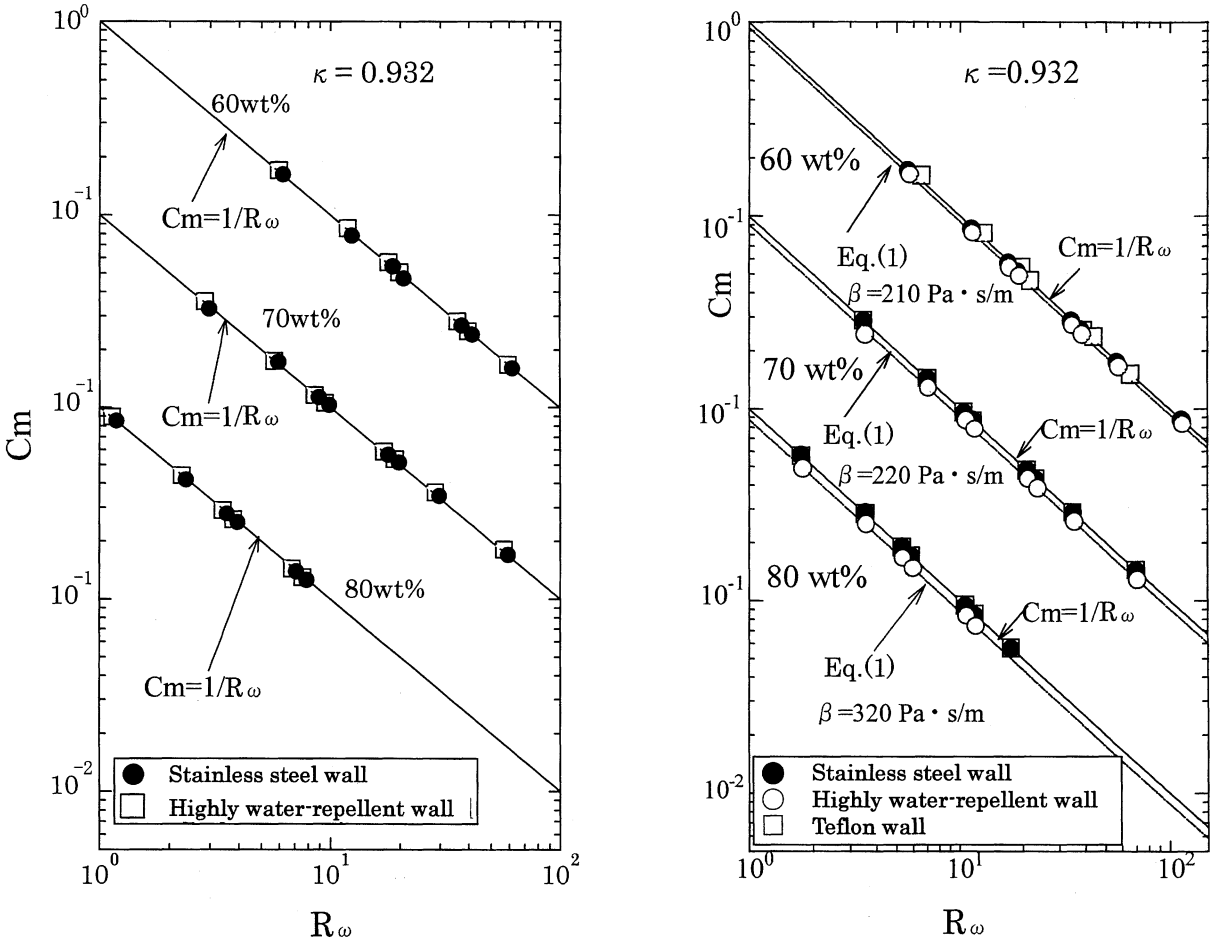

Figure 5. Moment coefficients for glycerin solutions.

ing the lengths and positions of the streak lines in the photographs, and these profiles were obtained when the surface of the inner rotating cylinder was wall No. 2 and when the outer stationary cylinder was clear acrylic. As learned from the moment measurements, drag reduction occurs with wall No. 2.

In a steady laminar Couette flow, the velocity in the θ-direction v is

$$v = \left[\left(\frac{r^2 - R_0^2}{R_0 r}\right)(\omega_i \kappa R_0 - V_s)\right] \Big/ \left(\kappa - \frac{1}{\kappa}\right) \qquad (3)$$

where r is the radius, ω_i is the angular speed of the inner cylinder, and V_s is the tangential slip velocity at the inner wall.

Velocity profiles when the inner cylinder was a smooth aluminum cylinder are shown in Figure 7. The Reynolds number, R_ω, was in the range of 10 to 25. In the figure, the solid lines are curves obtained by substituting $V_s = 0$ in Eq. 3. The experimental data cluster about the solid lines, with the amount of scatter being $\pm 5.0\%$. The results indicate that fluid slip does not occur at the cylinder wall with these glycerin solutions.

Velocity profiles for the wall No. 2 are shown in Figure 8. The effects of the radius ratio, κ, and of the glycerin concentration are shown in Figures 8a and 8b, respectively. In these figure parts, the dotted lines represent the velocity profiles for no slip, the same as the solid lines in Figure 7.

Figure 8 clearly shows that the fluid slips at the wall. In Figure 8a, the data show that the slip velocity is a maximum when the radius ratio is $\kappa = 0.839$, and in Figure 8b, the slip velocity is seen to increase with the glycerin concentration.

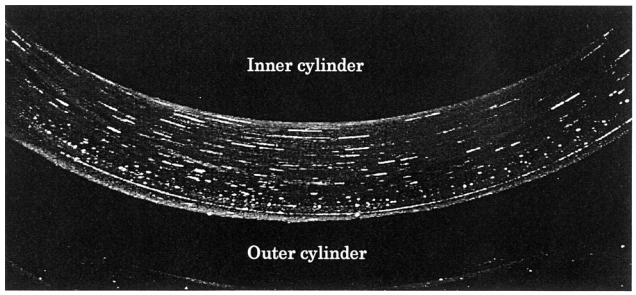

Figure 6. Flow between two cylinders, with the inner one rotating and the outer one at rest.

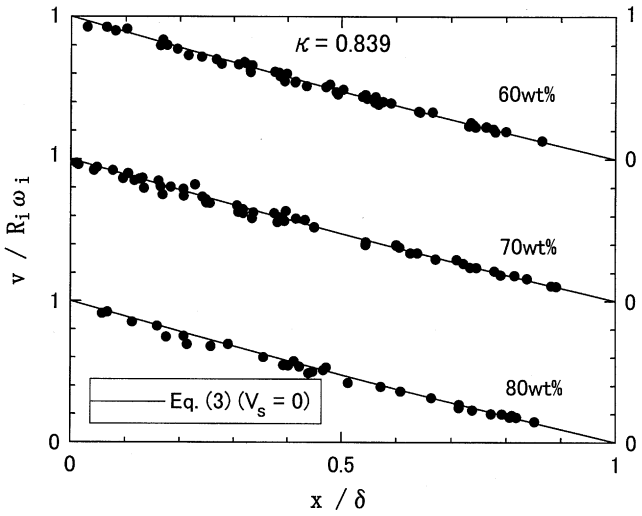

Figure 7. Velocity profiles for rotating smooth-wall inner cylinder.

The slip velocity was found by fitting Eq. 3 to the experimental data, and the values found are presented in Figure 9. The results there reveal that the maximum value of the slip velocity in this situation is less than 0.2, and that the slip velocity is weakly dependent on glycerin concentration and radius ratio.

We can use the velocity profiles to calculate drag reduction, and the resulting values are presented in Figure 10. The reduction increases with viscosity, and reaches a maximum when the radius ratio is $\kappa = 0.839$. The calculated values agree with the experimental result (Watanabe and Udagawa (2001) in order.

Flow visualization

When the speed of the inner cylinder reached a critical Reynolds number, the flow between the cylinders changed from a simple Couette flow to a Couette flow with Taylor cells. Since slip can have an effect on the Taylor cells, we carried out a numerical study of the Taylor vortex flow for the case of the highly water-repellent wall on the inner cylinder.

The numerical study was for the flow of an incompressible fluid with kinematic viscosity, ν, between two cylinders of height, L, and with inner radius, R_i, and outer radius, R_o. The three-dimensional (3-D) Navier–Stokes equations were taken as the governing equations for this study, which, for an axisymmetric flow, are

$$u\frac{\partial u}{\partial r} + w\frac{\partial u}{\partial z} - \frac{v^2}{r} = -\frac{\partial p}{\partial r} + \frac{1}{R\omega}\left(\frac{\partial^2 u}{\partial r^2} + \frac{1}{r}\frac{\partial u}{\partial r} - \frac{u}{r^2} + \frac{\partial^2 u}{\partial z^2}\right) \quad (4)$$

$$u\frac{\partial v}{\partial r} + w\frac{\partial v}{\partial z} + \frac{uv}{r} = \frac{1}{R\omega}\left(\frac{\partial^2 v}{\partial r^2} + \frac{1}{r}\frac{\partial v}{\partial r} - \frac{v}{r^2} + \frac{\partial^2 v}{\partial z^2}\right) \quad (5)$$

$$u\frac{\partial w}{\partial r} + w\frac{\partial w}{\partial z} = -\frac{\partial p}{\partial z} + \frac{1}{R\omega}\left(\frac{\partial^2 w}{\partial r^2} + \frac{1}{r}\frac{\partial w}{\partial r} + \frac{\partial^2 w}{\partial z^2}\right) \quad (6)$$

$$\frac{\partial u}{\partial r} + \frac{\partial w}{\partial z} + \frac{u}{r} = 0 \quad (7)$$

where u, v, and w are the velocity components corresponding to the r, θ, and z coordinates where p is the dynamic pressure, and where the Reynolds number, $R\omega$, is defined as $R_i\omega_i\delta/\nu$.

Using the Stokes stream function, Ψ, the velocity components u and w are

$$u = \frac{1}{r}\frac{\partial \psi}{\partial z}, \qquad w = -\frac{1}{r}\frac{\partial \psi}{\partial r} \quad (8)$$

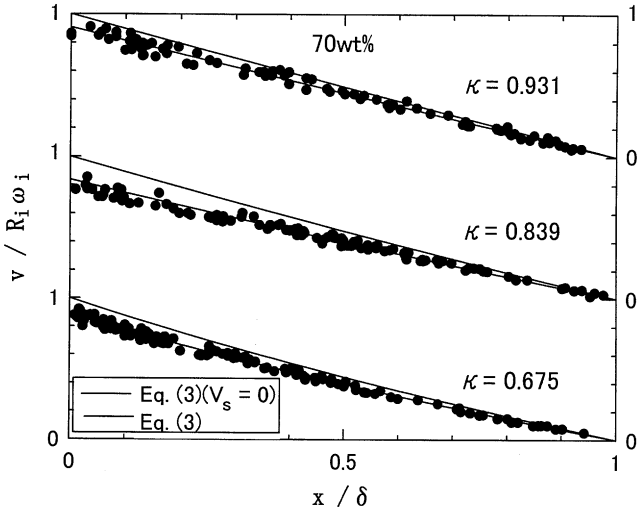

(A) Effect of radius ratio

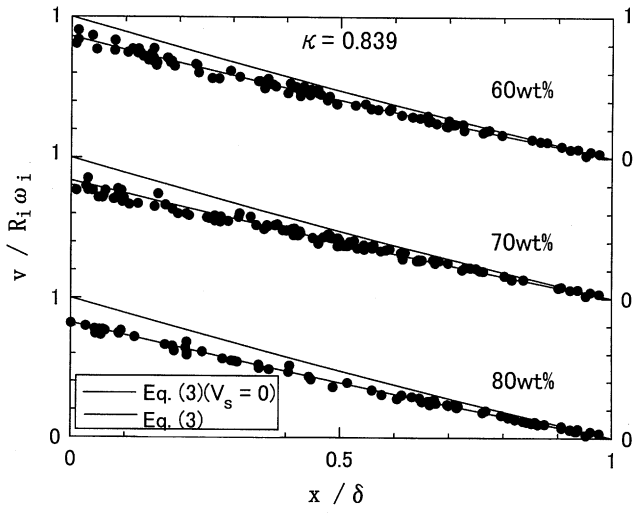

(B) Effect of concentration of glycerin solution

Figure 8. Velocity profiles for a highly water-repellent wall.

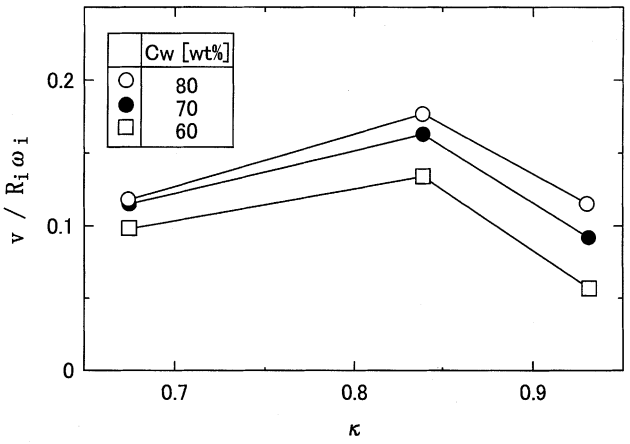

Figure 9. Slip velocities for glycerin solutions.

The boundary conditions are given as follows
For a smooth wall

$$u = w = 0, \quad v = R_i \omega_i \quad \text{at} \quad r = R_i$$
$$u = v = w = 0 \quad \text{at} \quad r = R_o \quad \text{and} \quad z = 0$$
$$\partial u/\partial z = \partial v/\partial z = 0, w = 0 \quad \text{at} \quad z = L/2$$

For a highly water-repellent wall

$$u = 0, \quad v = R_i \omega_i - V_s \; w = -W_s \quad \text{at} \quad r = R_i$$
$$u = v = w = 0 \quad \text{at} \quad r = R_o$$
$$\text{and} \quad z = 0$$
$$\partial u/\partial z = \partial v/\partial z = 0, w = 0 \quad \text{at} \quad z = L/2$$

where V_s and W_s are the slip velocities in the tangential and axial directions, respectively. These slip velocities were obtained by applying the Navier's boundary condition (Navier, 1816), that is

$$\tau_{r\theta}|_{r=Ri} = \beta V_s, \quad \tau_{rz}|_{r=Ri} = \beta W_s \tag{9}$$

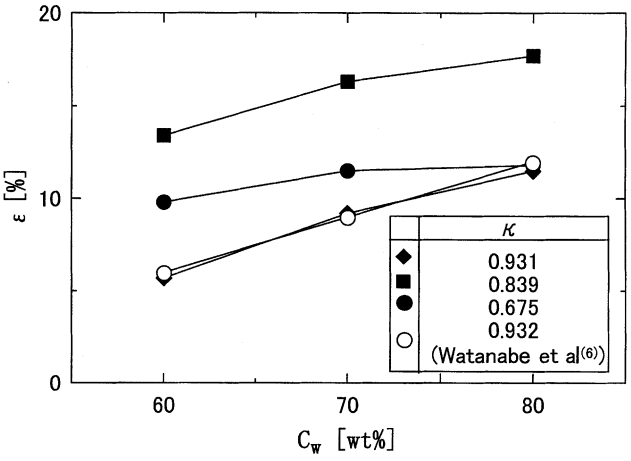

Figure 10. Drag reduction ratio for moment coefficient, calculated from the velocity profiles.

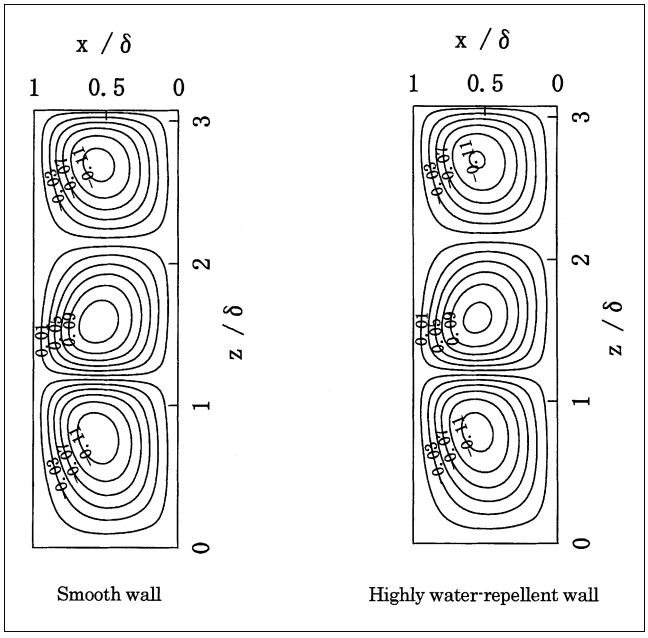

Figure 11. Numerical results; Taylor vortices ($\Gamma = 6.15$, $R_\omega = 300$).

Figure 11 shows stream lines obtained from the numerical work, and Figure 12 presents photographs of visualized Taylor cells. In both the numerical and visualization studies, the aspect ratio, Γ, is equal to 6.15. In the numerical work, the viscosity of the test fluid was that of the 80 wt % glycerin solution. In these figures, S. W and H. R. W indicate the smooth and highly water-repellent walls, respectively.

In Figure 11, three Taylor cells are shown in half of the cylinder length $z/\delta = 3.075$, and so there were six Taylor cells with smooth walls altogether in the annular flow. This number is in good agreement with the general flow pattern of Taylor vortex flow, in that the number of cells is an even number and approximately equal to the aspect ratio. And at the bottom of the annular space, the fluid moves from the outer cylinder to the inner cylinder. This result also agrees with many prior studies, for example, Benjamin (1979). When the inner cylinder has a highly water-repellent wall, number and flow direction of the Taylor cells are the same as in the case of the smooth wall. Comparing the size of the region where the absolute value of the stream function is high, the radius and axial velocity components for a highly water-repellent wall are smaller than those for a smooth wall.

In the photographs of Taylor cells in Figure 12, it is not related to the type of inner cylinder, and there are also three cells in the half-height, $l = 120$ mm. However, from these photographs, decreases in u and w, confirmed by the numerical analysis, cannot be confirmed, it is thought that the velocity components of a secondary flow may decrease from the reason for mentioning in the following.

The momentum equation for the radial direction is, without secondary motion

$$\frac{dp}{dr} = \frac{\rho}{r} v^2 \tag{10}$$

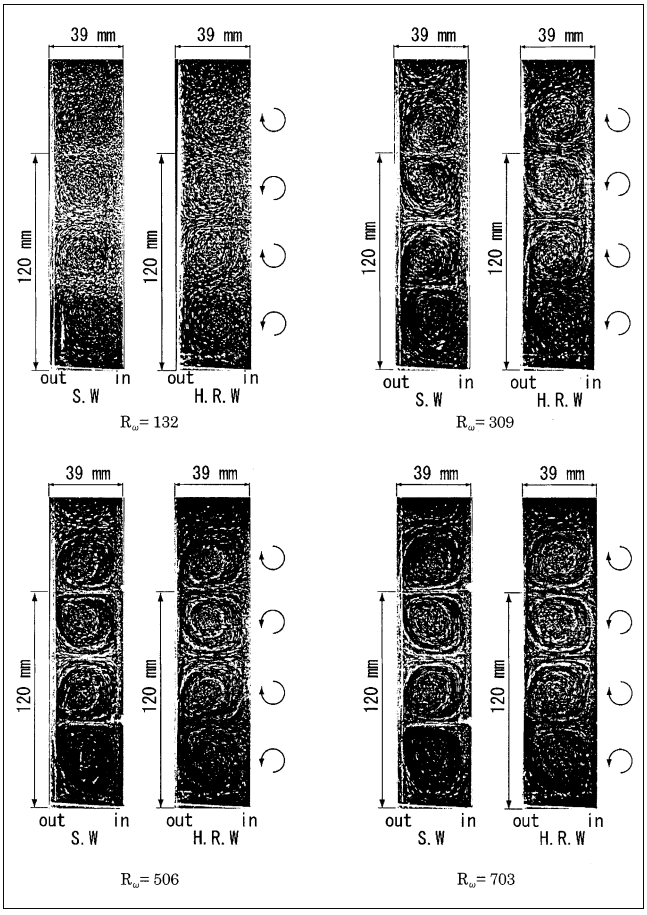

Figure 12. Taylor cells between rotating cylinders.

Substituting for v using Eq. 3, the solution of Eq. 10 is, with the boundary conditions of $p = p_i$ at $r = R_i$

$$\frac{p - p_i}{1/2\,\rho(R_i\omega_i)^2} = \left\{\frac{R_i\omega_i - V_s}{R_i\omega_i(\kappa - 1/\kappa)}\right\}^2 \times \left\{\frac{1}{R_o^2}(r^2 - R_i^2) - 4\ln\frac{r}{R_i} - R_o^2\left(\frac{1}{r^2} - \frac{1}{R_i^2}\right)\right\} \quad (11)$$

Figure 13 shows the results calculated using Eq. 11 for the case of Figure 12, where $\kappa = 0.675$ and where $R_\omega = 300$. The pressure gradient for the case of the highly water-repellent wall is lower than that of the smooth wall.

When the speed of the inner cylinder increases, and the flow becomes unstable, the velocity is not that given by Eq. 3. However, analogous to the results illustrated in Figure 13, the slip at the wall reduces the pressure gradient and, thus, weakens the flow of Taylor cells.

The height and the width of the cells were measured from photographs such as those in Figure 12. Figure 14 shows how the height varies with the Reynolds number, for three of the cells and for two surfaces. The cell that contacts the bottom of the cylinder is named Cell 1, the one alone is Cell 2, and so on. In Figure 14 there are differences in the heights for the two surfaces of the lower Reynolds numbers. For the

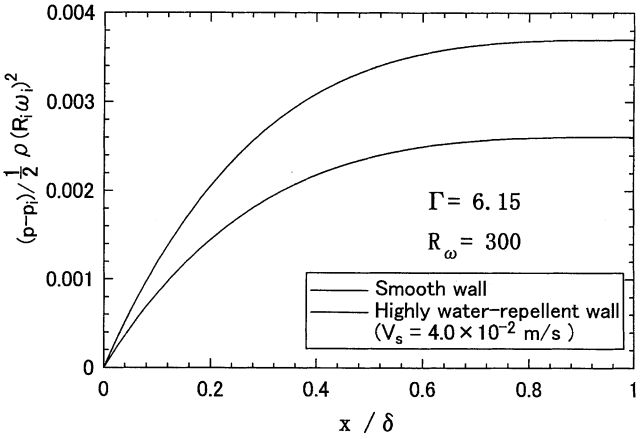

Figure 13. Variation of cell heights with Reynolds number.

highly water-repellent wall, the height of Cell 2 is higher (likewise Cell 1), but that of Cell 3 is lower. The actual differences in height were 1.3 mm (Cell 1), 1.6 mm (Cell 2), and 2.8 mm (Cell 3). The results of the numerical analysis, shown here for only Cell 1, also indicate a similar tendency of the experimental results.

It seems that the difference in height between two surfaces is related to fluid slip. Axial fluid slip is generated at the highly water-repellent wall. This slip causes the radius of the highly water-repellent inner cylinder to decrease on the appearance, in contrast with that of the smooth wall. Cells 1 and 2, which are received end face effect strongly, expands, so the heights of these cells are higher than that of the smooth wall. And the height of Cell 3 is decreased by the extension of Cells 1 and 2.

Figure 15 shows the effect of viscosity on the height of Cell 1. However, the change in the height of the cell is not dependent on the viscosity when the inner cylinder has a smooth wall, for the case of the highly water-repellent wall, however, the height of the cell is higher with the increase in the viscosity. Therefore the effect of fluid slip becomes remarkable as the viscosity increases. This tendency agrees well with the result of the measurement of the velocity distribution of the Couette flow.

Conclusions

The torque measurements made in this study show that drag reduction can be achieved in laminar Couette with a highly water-repellent wall, but only if the surface has fine grooves. This experimental result is consistent with the hypothesis developed from our previous study of pipe flow with a highly water-repellent wall, in which it was found that gas trapped in the grooves plays an important role in fluid slip.

Slip at the highly water-repellent wall is clearly identified from measurements of velocity close to the wall. The maximum slip was found to occur when the radius ratio κ was 0.839 in this experiment, and the maximum slip velocity was 18% of the wall velocity. The slip velocity is affected by the concentration of an increase in the radius ratio. The flow of Taylor cells becomes weak, so the slip velocity in the tangen-

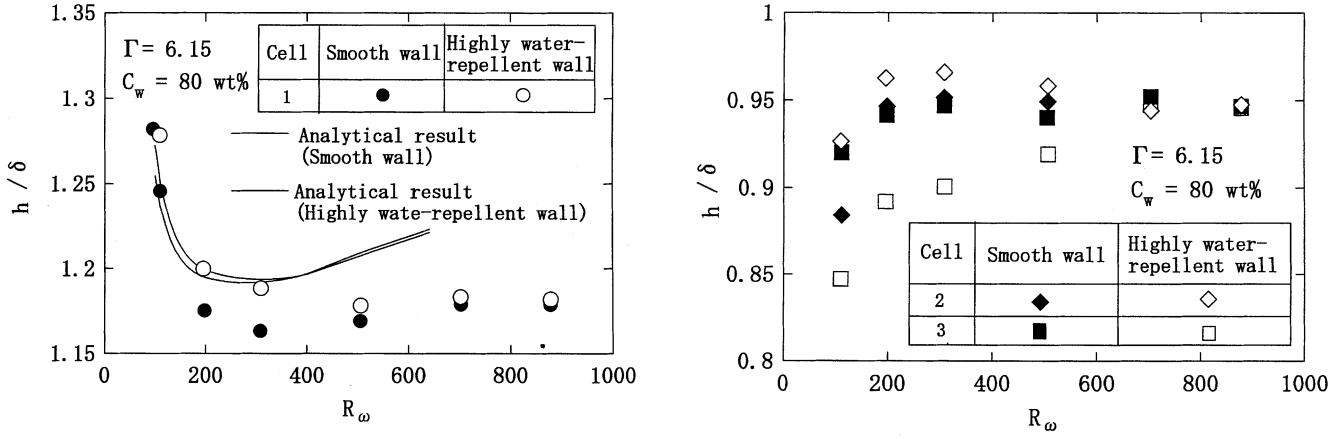

(a) Cell-1 (b) Cells 2 and 3

Figure 14. Variation of cell-1 heights with Reynolds number.

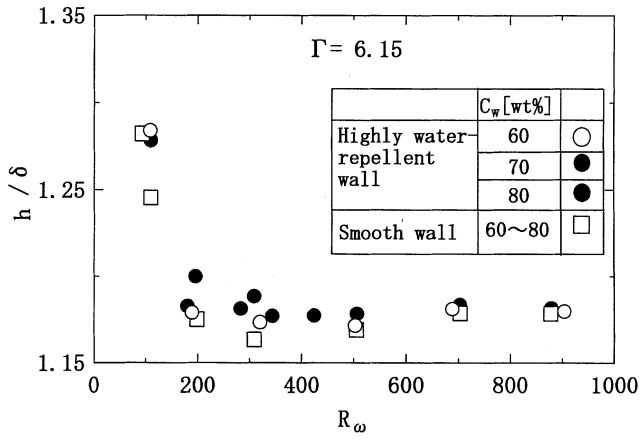

Figure 15. Variation of cell-1 heights with concentration of glycerin solution.

tial direction reduces the pressure difference between the two cylinders. The slip velocity of axial direction causes the difference in the size of the Taylor cells.

Acknowledgment

The authors acknowledge the financial support received from Grant-in-Aid for the Scientific Research Fund B (2), No. 12450075.

Notation

C_m = coefficient of torque $\{= T/2\pi\rho R_m^4 \omega_o^2 L\}$
C_w = concentration of glycerin solutions
l = distance from inner cylinder bottom
L = length of inner cylinder
p = dynamic pressure
p_i = dynamic pressure of inner cylinder
R_i = inner cylinder radius
R_m = mean radius $\{=(R_o + R_i)/2\}$
R_o = torque outer cylinder radius
R_ω = Reynolds number $\{ = (R_o - R_i)R_m \omega_o/\nu\}$
T = torque acting on inner cylinder
V_s = tangential slip velocity at wall
W_s = axial slip velocity at wall
x = distance from the wall of inner cylinder
u, v, w = velocity components

Greek letters

β = sliding coefficient
Γ = aspect ratio $\{= L/\delta\}$
Ψ = stream function
δ = gap $\{= R_o - R_i\}$
ϵ = drag reduction ratio
κ = radius ratio $\{= R_i/R_o\}$
μ = viscosity
ν = kinematic viscosity
ρ = density
τ_w = wall shear stress
ω_i = angular velocity of the inner cylinder
ω_o = angular velocity of the outer cylinder
r, θ, z = cylindrical coordinates

Literature Cited

Benjamin, T. B., "Bifurcation Phenomena in Steady Flows of a Viscous Liquid. II. Theory," *Philos. Trans. Roy. Soc. London*, **A359**, 27 (1979).

Navier, C. L.M. H., *Mem. Acad. Roy. Sci. Inst. Fr.*, **1**, 235 (1816).

Ogata, S., and K. Watanabe, "Flow Characteristics of a Drag Reducing Rotating Disk with Highly Water-Repellent Wall," *Proc. Joint ASME/JSME Fluid Engineering Conf*., p. 7 (1999).

Toms, B. A., "Some Observations on the Flow of Linear Polymer Solutions through Straight Tubes at Large Reynolds Number," *Proc. Int. Congr. on Rheology*, Vol. II, p. 135 (1948).

Watanabe, K. and S. Ogata, "Drag Reduction for a Rotating Disk with Highly Water-Repellent Wall," *JSME Int. J.*, **B41**(3), 556 (1998).

Watanabe, K., and T. Akino, "Drag Reduction in Laminar Flow Between Two Vertical Coaxial Cylinders," *Trans. ASME, Fluids Eng.*, **121**(3), 541 (1999).

Watanabe, K., and H. Udagawa, "Drag Reduction of Non-Newtonian Fluids in a Circular Pipe with a Highly Water-Repellent Wall," *AIChE J.*, **47**(2), 256 (2001).

Watanabe, K., Yanuar, and H. Udagawa, "Drag Reduction of Newtonian Fluid in a Circular Pipe with a Highly Water-Repellent Wall," *J. Fluid Mech*., **381**, 225 (1999).

Manuscript received May 21, 2002, and final revision received Feb. 18, 2003.